CHAPTER 45

Instabilities in the Longshore Current

N. Dodd[1], J. Oltman-Shay[2] and E.B. Thornton[3]

Abstract

Measurements made during one day of the 1986 SUPERDUCK experiment at Duck, North Carolina are used in order to investigate the model of Bowen & Holman (1989). This model explains low-frequency oscillations in the longshore current, which were observed during that experiment, in terms of a shear instability in that flow. The model is extended to include dissipation (in the form of bottom friction), and it is found that there is good agreement between it and observation.

1. Introduction.

During the 1986 Superduck experiment, at Duck, North Carolina, Oltman-Shay et al. (1989) noticed considerable along-shore progressive wave-like motions. These motions possessed periods of up to the order of 1000 seconds, and can therefore be described as low frequency. However, their associated wavelengths were of the order of 100 metres; this distinguishes them from infragravity waves which possess much longer wavelengths. Furthermore, they were only observed in the presence of a strong longshore current, which was a feature of most days of this experiment: when this current subsided, the oscillations were no longer apparent.

The measurements were made in about 1 to 2 metres of water, in the trough of the offshore bar which developed during the experiment. The incident swell had a period of about 5 seconds and approached the north-south tending beach at large angles. The longshore current was generated whcn these waves broke on the offshore bar. The waves then reformed and finally broke at the shore. Outside the surf zone, a corresponding long-time modulation of the incoming wave train was not noticed.

---

[1]Adjunct Research Professor, Oceanography Dept., Naval Postgraduate School, Monterey, CA 93943, U.S.A.

[2]Senior Scientist, Quest Integrated, Applied Physics Division, 21414 68th Avenue South, Kent WA 98032, U.S.A.

[3]Professor, Oceanography Dept., Naval Postgraduate School, Monterey, CA 93943, U.S.A.

Bowen & Holman (1989) have since presented a model, based on the inviscid, linear 2-dimensional shallow water equations, (under the rigid-lid assumption), to describe these motions. Their hypothesis is that these oscillations are manifestations of a shear instability in the along-shore shear flow (longshore current). This approach is in contrast with those of Symonds et al. (1982), Tang and Dalrymple (1989), and Shemer et al. (1990), all of whom assume low frequency nearshore motions to be forced phenomena.

In the analysis of Bowen & Holman, the mean longshore current is considered time independent and known a priori. The assumption of along-shore (y) uniformity is introduced, which allows the governing equations to be reduced to a single equation, analogous to the Rayleigh stability equation; the difference being due to the dependence of the water depth, h, on the cross-shore coordinate, x. Normal mode analysis then predicts a spectrum of eigenvalues/functions, each of which corresponds to a temporally stable or unstable perturbation, (or mode), of the shear flow. The authors assume the observed perturbations to be the fastest growing unstable modes, for a particular wavelength, λ; i.e. the unstable modes with the largest growth rates. The spectrum of eigenvalues/functions is defined by the cross-shore depth, ($h(x)$), and longshore current, ($V(x)$), profiles. The situation is depicted in figure 1. They supported their hypothesis by applying this model to a highly simplified set of profiles. Dodd & Thornton (1990) have since shown more rigorously that the model agrees with observation on the non-dispersive nature of the oscillations in frequency-wavenumber (f,k) space.

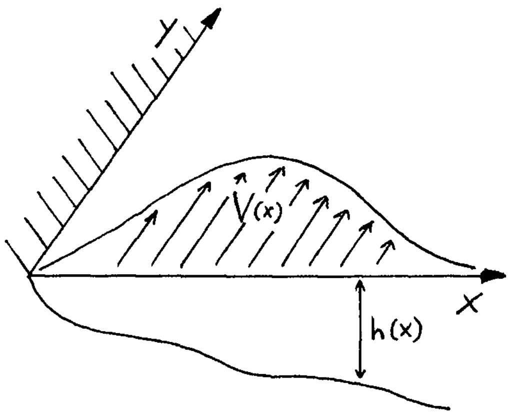

Figure 1. Nearshore bathymetry, $h(x)$, and longshore current, $V(x)$, and their relation to the coordinate system used.

In the following work we examine results from one day of the SUPERDUCK experiment, and we apply the model of Bowen & Holman to the measured V and h profiles for that day. Being a linear analysis, no information concerning the absolute amplitudes of these perturbations can be obtained. Therefore, we concentrate our efforts on comparing observed and predicted (f,k) spectra. In doing this it must be assumed that V and h are dependent only on the cross-shore coordinate, x. Though the bathymetry was mildly three-dimensional, this is a reasonable assumption.

2. Theoretical and Numerical Background.

We consider the domain $0 < x < \infty$, $-\infty < y < \infty$, with the shoreline situated at x=0. The total velocity vector, $\underline{u}^*$, is defined as

$$\underline{u}^* = (u(x,y,t), v(x,y,t) + V(x)). \tag{1}$$

Thus u and v represent the perturbed velocity field and V represents the longshore current. When (1) is introduced into the shallow water equations, which are linearized under the assumption $V_0 >> u_0$, (where V_0 is a representative amplitude of the longshore current and u_0 is a similar quantity for the perturbed velocity field), we get:

$$\begin{aligned} u_t + Vu_y &= -g\zeta_x \\ v_t + uV_x + Vv_y &= -g\zeta_y \end{aligned} \tag{2}$$

where t is the time coordinate, ζ is the free-surface elevation, and g is the gravitational acceleration constant. Under the rigid-lid assumption, a stream function, $\Psi(x,y,t)$, is introduced into (2), where $u = -\Psi_y/h$ and $v = \Psi_x/h$; this allows the equations (2) to be combined into a single equation. Making the further assumption that the along-shore behavior is simple harmonic, then

$$\Psi(x,y,t) = \Re\{\psi(x)e^{i(ky-\omega t)}\} \tag{3}$$

Thus, the cross-shore structure is described by $\psi(x)$. The resulting linearized equation is

$$(V-c)\{\psi_{xx} - (h_x/h)\psi_x - k^2\psi\} = h(V_x/h)_x\psi. \tag{4}$$

The wavenumber, k=$2\pi/\lambda$, is assumed to be real. The phase velocity, c, (and therefore the frequency, ω=ck), will in general be complex. Thus if c possesses a positive imaginary part, Ψ will be a temporally unstable mode, with wavelength $2\pi/k$, real radian frequency $\Re(\omega)$, and growth rate $\Im(\omega)$. One condition for there to be an instability is that the potential vorticity associated with the shear flow, V_x/h, should possess a local extremum. This condition is satisfied for all the profiles examined here.

In general, (4) must be solved numerically. Here we use a finite difference solution. In this scheme, (4) is discretized at N nodes on the domain $0 < i\Delta x < (N\text{-}1)\Delta x = L$, ($i$=1, .., N-2), where Δx is the distance between nodes, and L is some suitably large value. The scheme is accurate to $O(\Delta x^4)$, and the relevant finite-difference approximations for the derivatives in (4) can be found in Collatz (1960). At the boundaries, non-symmetric approximations are derived to the same order of accuracy, although it should be noted that the comparatively large coefficient of the truncation error term, due to the non-symmetric nature of the boundary conditions, degrades accuracy somewhat. The problem may then be posed as a generalized algebraic eigenvalue problem,

$$\boldsymbol{A}\underline{\psi} = c\boldsymbol{B}\underline{\psi}, \tag{5}$$

(where $\underline{\psi} = (\psi_0, ..., \psi_N)$, and $\psi_i = \psi(i\Delta x)$), and solved subject to the no-normal-flow boundary conditions: $\psi_0 = \psi_N = 0$. In fact, (5) may be solved more rapidly as a classical eigenvalue problem by operating on it with B^{-1}, which is easily calculated since B is well-conditioned. Such a solution yields N-1 eigenvalues, c_i, each with an associated eigenfunction, $\underline{\psi}_i$. This method of solution has the disadvantage of being computationally expensive, in both storage and cpu time, and of being generally less accurate than initial-value methods. It is usually used in order to generate initial estimates to eigenvalues, which can then be more accurately estimated using a shooting method. Here this method is used by itself, because the profiles we will be looking at are not smooth, analytic functions, but discrete and numerically generated. This severely restricts the usefulness of shooting methods for this problem. A value of N = 201 was the largest that the available storage and cpu time would allow on an IBM 3033. This was adequate for the investigation.

3. Bottom Friction.

The model presented in the preceding section neglects dissipative effects. However, such effects can be important in damping unstable modes. Bowen & Holman included a damping factor, $e^{-\nu t}$, in (3), and estimated that ν would be $O(10^{-2}\text{-}10^{-3}\ \mathrm{s}^{-1})$, implying that $\Im(\omega)$ must be larger than this for an instability to develop. In fact, dissipative effects can be included in the momentum equations on a rational basis. The equations (2) represent a decoupling of higher order effects, (i.e. perturbations in the longshore current), from the lowest order balance. This balance is between the radiation stress gradients, which are generated by waves breaking at a beach and which lead to the formation of a longshore current, and the bottom friction, and is discussed by Longuet-Higgins (1972). In the higher-order balance wave breaking is absent, and so the most significant dissipative effect is bottom friction. This effect may be included by adding an appropriate term to the momentum equations:

$$\begin{aligned} u_t + Vu_y &= -g\zeta_x - \mu u \\ v_t + Vv_y + V_x u &= -g\zeta_y - \mu v \end{aligned} \tag{6}$$

Thus the term μ represents the dissipation in the problem. It may be derived on the assumption that the amplitude of the orbital velocity of the incoming gravity wave, U_0, is much greater than the representative longshore velocity, V_0: i.e. $U_0 >> V_0$. Thus,

$$\mu = \frac{2}{\pi} c_D U_0 \tag{7}$$

where c_D is a dimensionless drag coefficient. (In fact, this assumption is invalid for Duck. Howevcr, it is the size of μ which is of importance hcrc and not its form). These equations can then be combined as before to give

$$(V - \frac{i\mu}{kh} - c)\{\psi_{xx} - (h_x/h)\psi_x - k^2\psi\} = h(V_x/h)_x\psi - \frac{i\mu}{kh}(h_x/h)\psi_x \tag{8}$$

It can be seen that μ is always accompanied by i (= $+(-1)^{1/2}$).

The equation (8) can be solved by the method already outlined in the previous section. It is this equation which will be applicd to measured V and h profiles from the SUPERDUCK experiment.

4. Observations.

We examine observations from onc day of the SUPERDUCK experimcnt, October 16th, which exhibited the most energetic low frequency motions. For a full description of the field site and the methods of data collection thc reader is referrcd to Oltman-Shay ct al. (1989).

Some of the strongest evidence presented by Oltman-Shay et al. for the existcnce of low frequency perturbations in the longshore current is in thc form of itcrative maximum likelihood estimated (IMLE) frequency-cyclic wavenumber (f,K) spectra, (where $K = k/2\pi$). Figure 2 shows one such diagram for Oct. 16th, which was constructed from the along-shore component of velocity as measured on that day. Note that the frequency is cut off at 0.05 Hz (20 seconds), thus excluding the incoming swell. The diagram therefore shows only low frequency motions, (compared to the incoming wave train). The figure shows theoretical edge wave dispersion lines for 0 mode and two higher mode edge waves (for a plane beach). Note that frcquency bins are now of width about $\Delta f = 0.001$ Hz, and are thus better resolved than the original figures of Oltman-Shay et al.; otherwise, the diagram is similar to those presented, (for other days), by Oltman-Shay et al.

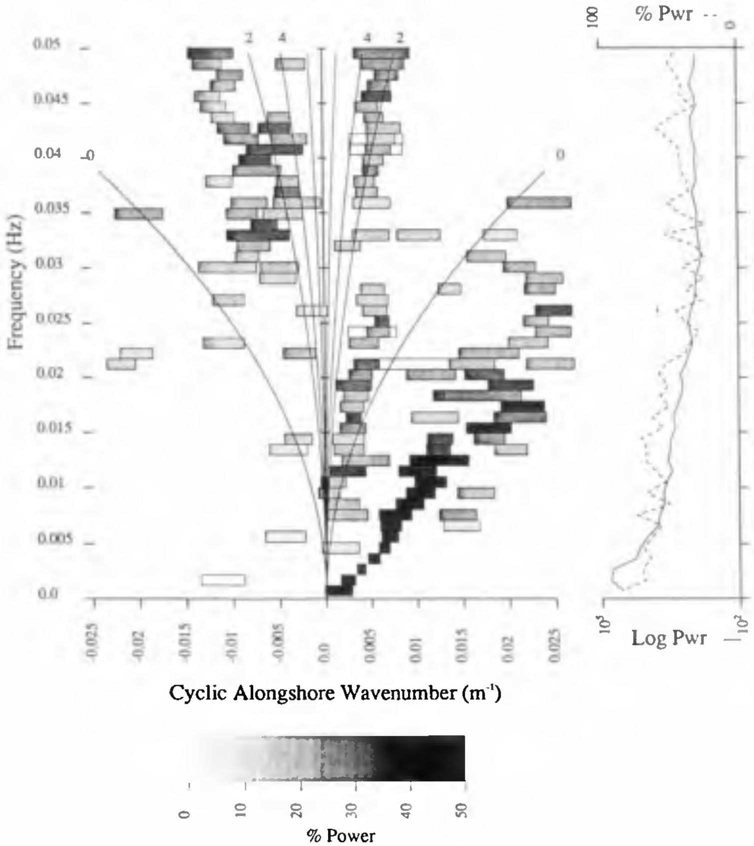

Figure 2. IMLE frequency-cyclic wavenumber spectrum of along-shore velocity on October 16th. Positive wavenumbers indicate southward propagation. Rectangular boxes indicate position of variance peaks defined as those wavenumber maxima having an adjacent valley below their half-power. The wavenumber width of each box is the half-power bandwidth of the peak. Shading density indicates the percent variance in the frequency bin that lies within the half power bandwidth of the peak. Theoretical edge wave dispersion curves (0, 2 and 4), and leaky-trapped boundary are shown. Log power density (cm^2/s, solid) and total percent variance displayed in the frequency-wavenumber spectrum (dashed) as a function of the frequency are shown alongside. $\Delta f = 0.00098$ Hz.

There is evidence of edge wave activity in the diagram, which is mostly restricted to frequencies above 0.01 Hz, though it is hard to tell which modes are present. This is partly due the array being too short to successfully resolve them. However, the shorter, low frequency motions do not suffer from this problem; in fact, the most well defined variance peaks lie well outside the edge wave dispersion curves, and below 0.015 Hz. They appear to describe a roughly linear relation between frequency and wavenumber. As Oltman-Shay et al. noted, these lines are not attributable to advected edge waves, (due to the longshore current), or to deviations of the edge wave dispersion curves from the theoretical form indicated on the figure, (due to deviations of the beach profile from its theoretically plane form). These oscillations can be seen to be progressive, with a phase speed of about 0.9 m/s. They are in the same direction as the longshore current on that day, the maximum value of which was about 1.2 m/s. On this and other days examined, the measured phase speeds were about one half to three quarters the corresponding maximum longshore current value. This is in agreement with theory.

5. Computations.

In order to use the model (8) the cross-shore bathymetry, $h(x)$, and longshore current profile, $V(x)$, must be constructed for October 16th. In the case of h this presents no problems, but for V things are not so simple. This is because there were very few measurements of longshore current made; in fact there are only five such measurements for the 16th. It is therefore difficult to know what the true profile is. However, small differences in this profile can substantially affect the predicted stability characteristics for that day. It is therefore important that we have reasonable confidence in the profile used. Another problem, which is linked to the first, is that the profile was measured sequentially, over a period of about four hours, as a sled was moved in a transect across the foreshore. Although this process was centered about low tide, the depth changed by about 0.2 m during the time the measurements were made. This, combined with other changes which may have occurred in the incoming wave field, may be enough to considerably affect the mean longshore current profile and thus render any profile interpolated from the measured profile dubious at best.

Unfortunately, there is little or no analytical work available for longshore current generation on a barred beach. Therefore, we use the model of Thornton & Whitford (1990) to generate a set of V profiles for the period during which the measurements were taken, to allow for the affects of tidal variations. There are five such profiles in all, (denoted cases A to E), each with an associated depth profile, which covered the tidal range. They are shown in figures 3(a) and 3(b). The actual measured values of V are also shown in figure 3(a). It can be seen that there is a fairly large difference between the first and the last profiles, (A and E), and that the measured values agree closely with profiles C and D. Case E is markedly different from the rest. Moving beach-ward from offshore, each profile is, however, qualitatively similar: there is a maximum in V, followed by a sharp decrease, then a slowing of the decrease, and finally a rapid decay to zero at the shoreline. The large peak in each profile is due to the waves breaking on the bar, and the slowing of the rate of decrease, (which results in a "kink" in the onshore shear), is a result of waves finally breaking at the shore. These features are typical of longshore current profiles on barred beaches. It is easy to see that merely interpolating from the measured values will lead to a qualitatively different profile. There will be no such secondary breaking modeled. The drag coefficient, c_D, was measured at about 0.003, and this value is used throughout the following analysis.

The profiles shown in figures 3(a) and 3(b) are now inserted into (8) and the resulting eigenvalue problem solved. Recall that it is the fastest growing unstable modes which will be of importance; other unstable modes may be present but the modes with the (a).

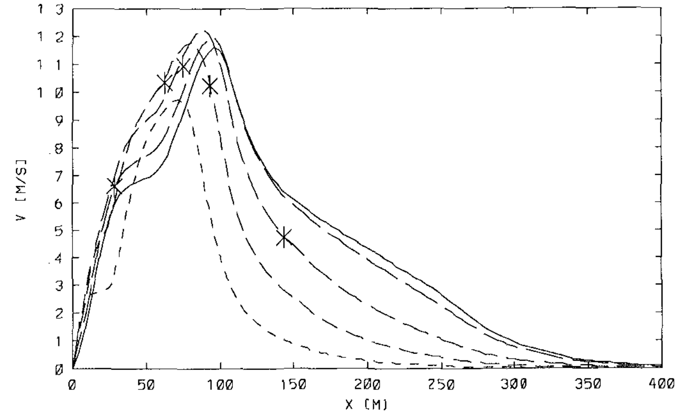

(b).

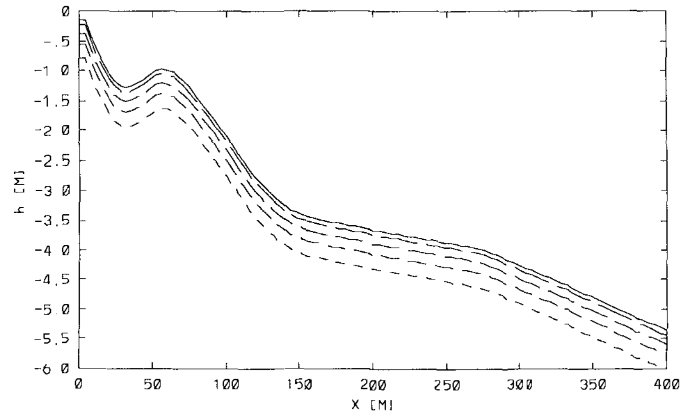

Figure 3. Longshore current (a). and depth (b). profiles used in the stability analysis. Case A is shown by the solid line and cases B to E by dashed lines with progressively shorter dash lengths. Measured longshore current values are indicated in 3(b) by an asterisk.

largest growth rates are expected to be apparent first. We denote the growth rates: $G = \Im(\omega)$. Each of these unstable modes possesses an associated real frequency, $F=\Re(\omega)/2\pi$. In figure 4 we compare the predicted frequencies with the measured frequency-cyclic wavenumber spectra. In this diagram the shading present in figure 2 is omitted so that the comparison can be seen more clearly.

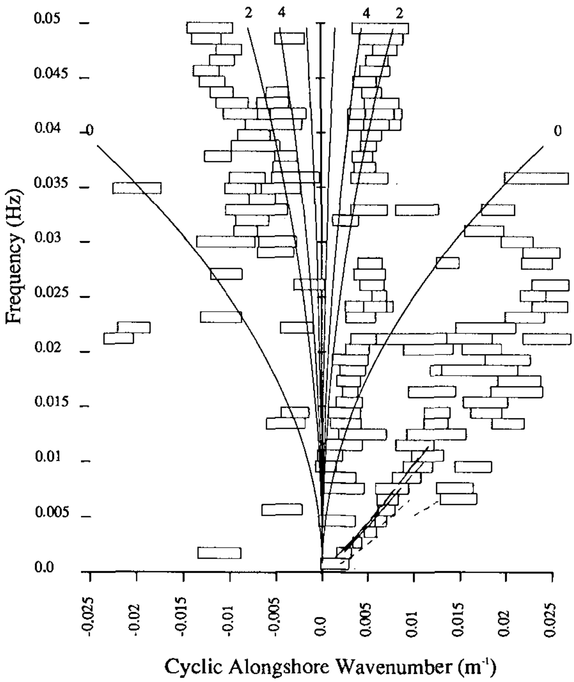

Figure 4. Reproduction of IMLE spectrum shown in figure 2, without shading. Also shown are the predicted dispersion curves, corresponding to the fastest growing unstable modes, for each of the cases A to E. Case A is shown as a solid line, and thereafter cases B to E are shown as dashed lines with progressively shorter dash lengths.

It can be seen that cases A to D give similar dispersion curves. They agree well with measurement. Case E differs substantially from these. Considering the aforementioned difference between this V profile and thc rest, this is not surprising. The dispersion curve predicted in this case agrees comparatively poorly with the measured spectra, and for these reasons we now discard case E. Note also that a number of the cases give discontinuous dispersion curves. In these cases, each segment of the curve corresponds to a different unstable mode (eigenvalue) from adjacent segments. They result from G increasing as K increases, for one mode, while for anothcr G decreases. Hence there is a "jump" from one mode to another as the growth rate of the latter exceeds that of the first.

It should be remembered that no information concerning the absolute amplitudes of these oscillations may be obtained from this linear analysis. Thus only relative intensities can be compared. The model of Bowen & Holman explains perturbations of a shear flow as instabilities in that flow. On this assumption it is natural to extend this interpretation to explain more vigorous perturbations as more unstable modes; i.e. modes with larger growth rates. To make this comparison the IMLE diagram shown in figure 2 is rescaled. In the original figure degrees of shading represent wave energy at a particular wavenumber as a percentage of total energy in that frequency bin. In figure 5, although the original IMLE "boxes" are retained, the shading now represents absolute variance, (or energy), thus allowing comparisons between different frequencies to be made.

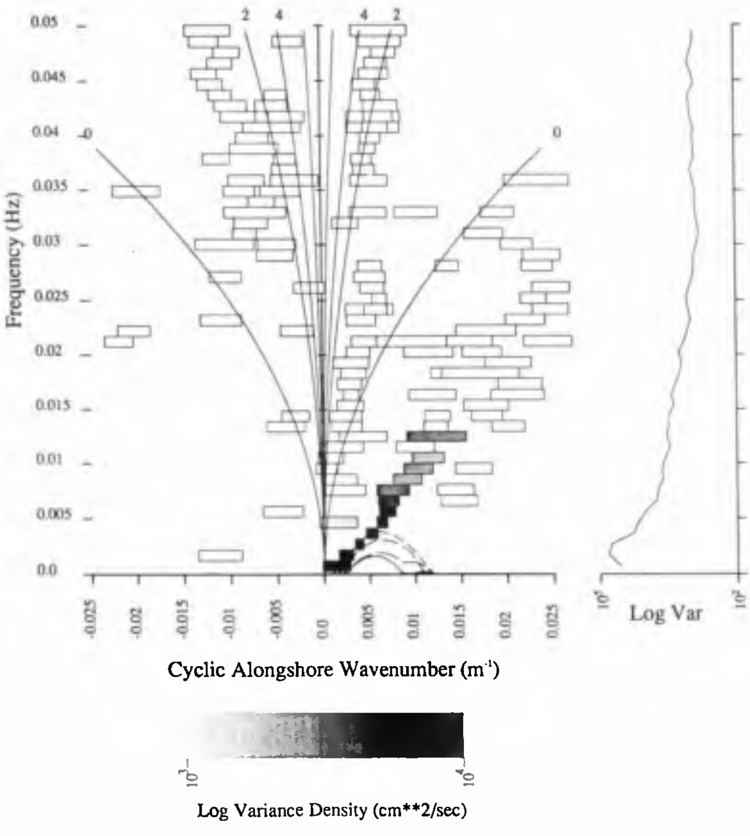

Figure 5. IMLE frequency-cyclic wavenumber spectrum for along-shore velocity, on October 16th. Shading indicates absolute log variance density. Log variance density in the frequency-cyclic wavenumber spectrum as a function of frequency is shown alongside. $\Delta f = 0.00098$ Hz. Also shown are the predicted growth rates, G, (units, rad/s) for the cases A to D. A is shown by the solid line, and B to D by dashed lines with a progressively decreased dash length.

In this figure, measured variance is virtually all concentrated below 0.01 Hz, showing that these motions are far more energetic than any other low frequency motions. In the accompanying log variance plot, the variance can be seen to increase, from very low frequencies, up to a peak in the second frequency bin, (about 0.001 to 0.002 Hz), and decrease thereafter.

The predicted growth rates, G, are shown in the same diagram, (excluding case E). Each of these shows an increase in G, from low wavenumbers, and frequencies, (see the corresponding frequencies in figure 4), to a peak growth rate, and then a decrease as K increases further. This is in rough agreement with the observed spectra. The main area of disagreement is at very small wavenumbers, (very low frequencies), where theory predicts no instability, but quite energetic motions were measured. As we proceed from case A through to case D, the maximum growth rates of the predicted instabilities becomes larger. That this is not solely due to differences in the V profiles can be discovered by re-solving the eigenvalue problem (8) using the longshore current profile for case A and the depth profile for case E. Larger growth rates are found for this case than for case A alone.

6. Discussion and Conclusions.

The further analysis of the observations made on one day of the SUPERDUCK experiment provides some further support for the hypothesis of Bowen & Holman: these motions are manifestations of a shear instability in the longshore shear flow. The improvement in resolution of the IMLE spectrum shown here, (Δf=0.00098 Hz as opposed to 0.002 Hz), clearly indicates the presence of these motions, lying in a straight line. They also clearly dominate other wave activity. They also reveal the existence of a peak in the energy of these motions, (lying between 0.001 and 0.002 Hz). Theory concurs. The predicted dispersion lines agree well with observation. The results for the 16th are typical for those on other days.

There are some notable discrepancies however. The range of the predicted instability, though in general agreement with measurment, is not the same, and in particular, energetic motions at very low frequencies and wavenumbers are shown by the measurements, and these are not predicted by the theory. These discrepancies may be explained by the fact that there is, in each case, more than one unstable mode. The existence of the motions at larger frequencies may be a result of interactions between such modes. Dodd et al. (1990) have also shown strong evidence of an offset (non-zero intercept) of the linear dispersion lines in IMLE spectra constructed from the cross-shore component of velocity. They thought that this could be caused by the existence of a rip current, and this could explain the existence of intense motions at very low frequencies. Dissipation, as modeled here, appears to be play the important role of damping unstable modes with very small growth rates. This is in agreement with Bowen & Holman.

Finally, we consider the stream function, ψ. For case A, the unstable mode with the maximum growth rate exists at about K=0.006 m^{-1}; see figure 5. At this wavenumber another unstable mode exists. It is not shown in figure 5 because its growth rate, for this value of K, is smaller than that of the first mode by a factor of about 5. The growth rates shown in figure 5 are, of course, the eigenvalues in the problem (8), and with each of these is associated an eigenfunction. We denote these ψ_1 for the fastest growing mode (at K=0.006 m^{-1}), and ψ_2 for the second. In figure 6, we show $|\psi_1|^2$ and $|\psi_2|^2$ as functions of x. Also shown in this figure is the cross-shore potential vorticity profile (V_x/h) defined by case A. Note that the peaks in $|\psi_1|^2$ and $|\psi_2|^2$ occur in different places: the first at the local maximum in V_x/h, and the second at the second local minimum. Looking at figures 3(a) and 3(b), it can be seen that the minimum is associated with the offshore facing shear in V, and that the maximum is associated with the onshore facing shear. Specifically it is due to the "kink" in the V profile due to waves breaking at the shore. If this kink is removed, then the most unstable mode, ψ_1, disappears, leaving ψ_2 as the most unstable mode. This can be tested by either redefining the V profile between about x = 40 m and 100m, or by cubic interpolation between the measured V values shown in figure 3(a). A little further smoothing results in stability; i.e. the problem defined by (4) may be unstable, but the dissipative effects included in (8) damp such instabilities, since the growth rates associated with them are very small. All of this is also true of cases B, C and D. What it seems to indicate is that the instabilities associated with the longshore current profile at a barred beach are due specifically to the form of the onshore shear, and not the offshore (or back) shear, as first suggested by Bowen & Holman (1989).

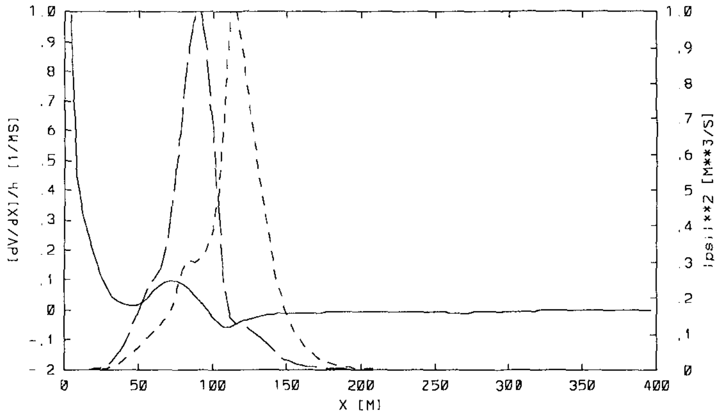

Figure 6. Potential vorticity of shear flow case A (solid line, left scale) and $|\psi_1|^2$ and $|\psi_2|^2$, (moduli squared of the stream functions of the first and second fastest growing modes in case A for K = 0.006 m^{-1}) (long and short dashed lines respectively, right scale) as functions of x.

7. Acknowledgments.

The work by N. Dodd and E.B. Thornton was direct funded by the Naval Postgraduate School under sponsorship of the Office of Naval Research. J. Oltman-Shay was funded by Office of Naval Research grant N00014-90-J-1118.

References.

Bowen, A.J. & R.A. Holman. 1989. Shear Instabilities of the Mean Longshore Current: 1. Theory. *J. Geophys. Res.*, 94, 18023-18030.

Collatz, L. 1960. The Numerical Treatment of Differential Equations. Springer-Verlag. 568p.

Dodd, N. & E.B. Thornton. 1990. Growth and Energetics of Shear Waves in the Nearshore. *J. Geophys. Res.*, (to appear).

Dodd, N., J. Oltman-Shay & E.B. Thornton. 1990. Instabilities in the Longshore Current: A Comparison of Theory and Observation. (Submitted to *J. Geophys. Res.*).

Longuet-Higgins, M.S. 1972. Recent Progress in the Study of Longshore Currents. In Waves on Beaches and Resulting Sediment Transport, 203-248. ed. R.E. Meyer. Academic Press.

Oltman-Shay, Joan, P.A. Howd and W.A. Birkemeier. 1989. Shear Instabilities of the Mean Longshore Current: 2. Field Observations.

Thornton, E.B. & D.J. Whitford. 1990. Longshore currents over a barred beach, I. Field experiment. (Submitted to *J. Phys. Ocean.*).